3D FE simulation of PISA monopile field tests at Dunkirk using SANISAND-MS

Pisanò, F.; Del Brocco, I.; Ho, H.M.; Brasile, S.

DOI
10.1680/jgele.23.00073

Publication date
2024

Document Version
Final published version

Published in
Geotechnique Letters

Pisanò, F. *et al*. (2024) ***Géotechnique Letters* 14**, 35–45, https://doi.org/10.1680/jgele.23.00073

3D FE simulation of PISA monopile field tests at Dunkirk using SANISAND-MS

F. PISANÒ*†, I. DEL BROCCO‡, H. M. HO§ and S. BRASILE‡

This paper presents an investigation into the suitability of the SANISAND-MS model for the three-dimensional finite-element (3D FE) simulation of cyclic monopile behaviour in sandy soils. In addition to previous work on the subject, the primary focus of this study is to further assess the model's capability to reproduce the accumulation of permanent deflection/tilt under cyclic lateral load histories. To this end, experimental data from the PISA field campaign are employed, particularly those emerged from the medium-scale cyclic tests conducted at the Dunkirk site in France. The methodology adopted herein involves calibrating the SANISAND-MS model's parameters to align with 3D FE simulation of a selected monotonic pile test reported by the PISA team using a bounding surface plasticity model partly similar to SANISAND-MS. Subsequently, the soil parameters governing SANISAND-MS' ratcheting response are calibrated using only minimal information from published PISA field data. While representing the first attempt to simulate the reference data set using a fully 'implicit' 3D FE approach, this paper offers novel insights into calibrating and using advanced cyclic models for monopile analysis and design – particularly, with regard to the quantitative influence of pile installation effects and sand's microstructural evolution under drained cyclic loading.

KEYWORDS: constitutive relations; finite-element modelling; repeated loading

NOTATION

A_0	SANISAND-MS 'intrinsic' dilatancy parameter
b_0	SANISAND-MS hardening factor
b^M	yield-to-memory surface distance in SANISAND-MS
b_{ref}	reference distance for normalisation in SANISAND-MS
C_e	high-cycle accumulation (HCA) model parameter governing void ratio effects
C_{N1}	first HCA model parameter governing cyclic preloading effects
C_{N2}	second HCA model parameter governing cyclic preloading effects
C_{N3}	third HCA model parameter governing cyclic preloading effects
C_p	HCA model parameter governing mean effective stress effects
C_U	uniformity coefficient
C_Y	HCA model parameter governing average stress ratio effects
C_δ	small dimensionless quantity
c	compression-to-extension strength ratio in SANISAND-MS
c_h	SANISAND-MS hardening parameter
D	outer pile diameter
D_{50}	sand's median grain size
D_r	relative density
e	void ratio
e_0	critical state line (CSL) void ratio intercept at $p' = 0$ kPa in SANISAND-MS
e_{ini}	initial void ratio
e_{max}	maximum void ratio
e_{min}	minimum void ratio
f_{shr}	memory surface shrinkage geometrical factor in SANISAND-MS
G_0	SANISAND-MS dimensionless small-strain shear modulus parameter
G_{max}	small-strain shear modulus
H	external lateral load
H_{max}	maximum lateral load within cyclic load set (LS)
h	hardening factor in SANISAND-MS
h_0	SANISAND-MS hardening parameter
h_e	lateral load eccentricity above ground surface
K_0	earth pressure coefficient
K_p	plastic modulus in SANISAND-MS
L	pile embedment length
M_b	SANISAND-MS bounding ratio in triaxial compression
M_c	SANISAND-MS critical stress ratio in triaxial compression
m	SANISAND-MS yield surface size parameter
m^M	memory surface size in SANISAND-MS
N	number of loading cycles
$\boldsymbol{n}$	unit tensor normal to yield surface in SANISAND-MS
$n^{b,d}$	SANISAND-MS bounding and dilatancy surface contraction/expansion parameters
p'	mean effective stress
p_{atm}	atmospheric pressure
pwp	pore-water pressure
q	deviatoric stress
$\boldsymbol{r}_{1,2,3}$	principal stress ratio axes
$\boldsymbol{r}_\alpha^M$	image back-stress ratio on memory surface along $\boldsymbol{n}$ in SANISAND-MS
$\tilde{\boldsymbol{r}}_\alpha^M$	image back-stress ratio on memory surface along $-\boldsymbol{n}$ in SANISAND-MS
t	pile wall thickness
U	pile head deflection at ground surface
U_R	accumulated pile head deflection at ground surface (relative to first cycle in load set)
$\boldsymbol{\alpha}$	back-stress ratio tensor in SANISAND-MS
$\boldsymbol{\alpha}^{b,c,d}$	image back-stress ratio on bounding, critical, dilatancy surfaces along $\boldsymbol{n}$ in SANISAND-MS
$\tilde{\boldsymbol{\alpha}}^{b,d}$	image back-stress ratio on bounding and dilatancy surfaces along $-\boldsymbol{n}$ in SANISAND-MS
$\boldsymbol{\alpha}_{in}$	initial load-reversal back-stress ratio tensor in SANISAND-MS
$\boldsymbol{\alpha}^M$	memory back-stress ratio tensor in SANISAND-MS
β	SANISAND-MS dilatancy memory parameter
ε_{ax}	axial strain

Manuscript received 27 August 2023; accepted 21 May 2024.
First published online 13 June 2024.
*Norwegian Geotechnical Institute, Boston, USA.
†Delft University of Technology, Netherlands.
‡Seequent, The Bentley Subsurface Company, Netherlands.
§Seequent, The Bentley Subsurface Company, Singapore.

ε_{vol} volumetric strain
ε_{vol}^{inst} enforced installation volumetric strain
ν Poisson's ratio
θ stress Lode angle
ζ SANISAND-MS memory surface shrinkage parameter
ζ_b cyclic stress amplitude factor
Λ plastic multiplier
λ_c SANISAND-MS CSL shape parameter
μ_0 SANISAND-MS ratcheting-control parameter
ξ SANISAND-MS CSL shape parameter
ψ state parameter
ψ^{acc} accumulated pile head rotation at the ground surface (relative to first cycle in LS)

INTRODUCTION

Monopiles are the most common type of foundation used for offshore wind turbines in water depths of up to approximately 50 m. To accommodate the increasing size of wind towers, monopiles with larger diameters (up to 8–10 m and beyond) are being adopted in the construction of modern offshore wind farms. The trend towards bigger turbines and support structures has accompanied the development of the offshore wind industry over the past decade, with a strong emphasis on reducing material costs through optimised design of structures and foundations.

Due to their widespread use, monopiles have been – and continue to be – at the core of important geotechnical research initiatives. Recent studies have focused on various aspects of monopile performance, including drivability and assessment of different installation methods (Byrne *et al.*, 2018; Achmus *et al.*, 2020), lateral capacity and stiffness (Byrne *et al.*, 2019; Jeanjean *et al.*, 2022; Maatouk *et al.*, 2022), interaction with difficult geomaterials such as chalk and glauconitic soils (Jardine *et al.*, 2019; Westgate *et al.*, 2023) and, more recently, dynamic/seismic response (Kaynia, 2019; Kementzetzidis *et al.*, 2021; Panagoulias *et al.*, 2023; Pisanò *et al.*, 2024). However, the assessment of monopile serviceability under cyclic loading conditions, particularly in terms of predicting lateral deflection/tilt accumulation, remains a subject of debate (Achmus *et al.*, 2009; Byrne *et al.*, 2020a; Page *et al.*, 2021; Staubach *et al.*, 2022; Pisanò *et al.*, 2022). While the offshore industry often requires simplified approaches (such as $p-y$ methods) for repetitive, location-specific calculations, advanced physical and numerical modelling study continues to be carried out to inform the development of simplified design methods (Klinkvort *et al.*, 2018; Pisanò, 2019).

This paper takes further recent research on the three-dimensional finite-element (3D FE) modelling of cyclically loaded monopiles using the SANISAND-MS model (Liu & Pisanò, 2019; Liu *et al.*, 2019) – that is, based on the step-by-step simulation of the foundation response to an external load history prescribed in the time domain. Using the terminology of Niemunis *et al.* (2005), this approach is henceforth referred to as 'implicit' – as opposed to 'explicit', which indicates analyses where loads and response variables are described/calculated as a function of the number of cycles. SANISAND-MS is a critical state, bounding surface plasticity model, built on the existing Sanisand formulation by Dafalias & Manzari (2004) and enriched with a so-called 'memory surface' to enhance the simulation of cyclic sand ratcheting (Corti *et al.*, 2016) (which is key to capturing the tilting behaviour of monopiles). Following previous computational studies on 3D FE monopile modelling (Liu *et al.*, 2022a, 2022b; Li *et al.*, 2023), this study seeks to confirm the suitability of the SANISAND-MS 3D FE approach by comparing numerical simulation results to selected field data from the literature. Specifically, new 3D FE SANISAND-MS results are benchmarked against the cyclic experimental test results obtained in dense marine sand at Dunkirk (France), and reported by Beuckelaers (2017) and Byrne *et al.* (2020b) as part of the PISA joint industry project. While the results of the main monotonic load tests have been thoroughly analysed through three-dimensional and one-dimensional monopile-soil modelling (Burd *et al.*, 2020; McAdam *et al.*, 2020; Taborda *et al.*, 2020), this paper tackles the implicit 3D simulation of the cyclic pile response.

Despite the challenges associated with capturing real (and partly unknown) field conditions and simulating the effects of long cyclic loading histories, the following results provide new evidence of the strengths and limitations of the 3D FE SANISAND-MS framework. After describing the steps taken to set up and calibrate the 3D FE numerical model, special attention is devoted to assessing its simulation capabilities and discussing the impact of relevant geotechnical factors, such as post-installation soil state.

SANISAND-MS MODEL: KEY MODEL FEATURES

The SANISAND-MS model was originally proposed by Liu *et al.* (2019) to improve the simulation of cyclic sand ratcheting with respect to the existing Sanisand parent model by Dafalias & Manzari (2004). Since the release of the initial version of SANISAND-MS, significant efforts have been devoted to developing a robust implementation for 3D FE simulations. The most recent set of model equations, which are utilised in this study, are described by Li *et al.* (2024) along with a demonstration of their positive impact on the quality of cyclic 3D FE simulation results.

SANISAND-MS is formulated in the framework of bounding surface plasticity and complies with well-established critical state theory principles using the state parameter ψ proposed by Been & Jefferies (1985). Following the work of Corti *et al.* (2016), the 'memory surface' concept has been cast into the Sanisand constitutive formulation to enhance the simulation of cyclic strain accumulation (cyclic ratcheting). As shown in Fig. 1, SANISAND-MS features four main model surfaces – namely, bounding, yield, dilatancy and memory surfaces. Notably, the memory surface enables phenomenological representation of micro-mechanical effects associated with fabric changes occurring during cycling, reflected at the macroscopic level by variations in stiffness and dilatancy.

In SANISAND-MS the evolution of sand stiffness in the elasto-plastic regime is determined both by the bounding and memory surfaces through the following formulation of the plastic modulus K_p:

$$K_p = \frac{2}{3} p' h \left(\boldsymbol{\alpha}^b - \boldsymbol{\alpha} \right) : \boldsymbol{n} \tag{1}$$

where p' is the mean effective stress and $(\boldsymbol{\alpha}^b\text{-}\boldsymbol{\alpha}) : \boldsymbol{n}$ quantifies the distance between the back stresses associated with bounding and yield surfaces ($\boldsymbol{\alpha}^b$ and $\boldsymbol{\alpha}$), after projection along the unit tensor normal to the yield surface, $\boldsymbol{n}$ (Fig. 1). In equation (1) the hardening coefficient h is defined as

$$h = \frac{b_0}{(\boldsymbol{\alpha} - \boldsymbol{\alpha}_{in}) : \boldsymbol{n} + C_\delta} \exp\left[\mu_0 \sqrt{\frac{p'}{p_{atm}}} \left(\frac{b^M}{b_{ref}} \right)^2 \right] \tag{2}$$

where – see Fig. 1 and Liu *et al.* (2019)]:

- $b_{ref} = \left(\boldsymbol{\alpha}^b - \widetilde{\boldsymbol{\alpha}}^b \right) : \boldsymbol{n}$, $b^M = (\boldsymbol{r}_\alpha^M - \boldsymbol{\alpha}) : \boldsymbol{n}$ accounts for the distance between memory and yield loci – with $\boldsymbol{r}_\alpha^M = \boldsymbol{\alpha}^M + \sqrt{2/3}\left(m^M - m\right)\boldsymbol{n}$ – and C_δ is a small dimensionless quantity (typically in the order of 10^{-3}) that prevents computational difficulties possibly caused by vanishing $(\boldsymbol{\alpha} - \boldsymbol{\alpha}_{in}) : \boldsymbol{n}$.
- the factor $b_0 = G_0 h_0 (1 - c_h e) / \sqrt{p'/p_{atm}}$ depends on the current void ratio (e) and mean effective stress, with G_0,

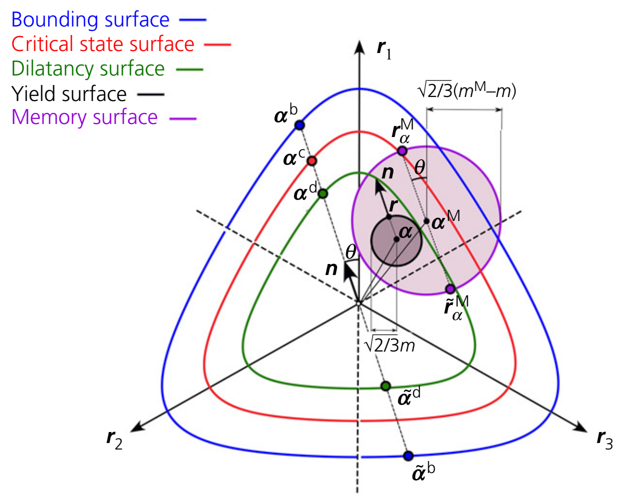

Fig. 1. SANISAND-MS model loci in the π plane

h_0 and c_h being dimensionless constitutive parameters.

- m^M and m are related to the radii of, respectively, the memory and yield surfaces, while μ_0 is a model parameter governing cyclic strain accumulation (ratcheting).
- $\boldsymbol{\alpha}_{in}$ is the $\boldsymbol{\alpha}$ value at the onset of a load reversal – that is, whenever the condition $(\boldsymbol{\alpha} - \boldsymbol{\alpha}_{in}) : \boldsymbol{n} < 0$ is fulfilled under any stress path.

The main effect of the memory mechanism is expressed by the exponential term in equation (2): an increase in the distance b^M determines larger plastic stiffness, while $b^M = 0$ (i.e. yield surface tangent to the memory locus) deactivates memory effects in the cyclic response.

The evolution laws for the internal variables m^M (memory surface size, equation (3)) and $\boldsymbol{\alpha}^M$ (memory back stress, equation (4) are key to the simulation of cyclic behaviour. As contractive behaviour promotes 'fabric reinforcement', stages of cyclic contraction are linked to an expansion of the memory surface ($dm^M > 0$), and therefore to larger stiffness through equations (1) and (2). Further, equation (3) also includes a competing memory-shrinking mechanism ($dm^M < 0$) to reproduce the loss in stiffness that may be caused by stages of dilative deformation:

$$\mathrm{d}m^M = \sqrt{\frac{3}{2}}\mathrm{d}\boldsymbol{\alpha}^M : \boldsymbol{n} - \frac{m^M}{\zeta} f_{shr} \langle -\mathrm{d}\varepsilon_v^p \rangle \tag{3}$$

where f_{shr} is a geometrical shrinkage factor (Liu *et al.*, 2019), while the material parameter ζ governs the memory surface shrinkage during dilation. The kinematics of the memory back stress $\boldsymbol{\alpha}^M$ follows directly from a parallel consistency condition imposed with respect to the memory surface:

$$\mathrm{d}\boldsymbol{\alpha}^M = \frac{2}{3}\langle \Lambda \rangle h^M \left(\boldsymbol{\alpha}^b - \boldsymbol{r}_{\alpha}^M \right) \tag{4}$$

In comparison to Liu *et al.* (2019), minor modifications to certain constitutive equations have been introduced to improve the numerical performance under complex stress paths, including model loci featuring π-sections based on Van Eekelen (1980) (Fig. 1), a slight modification of the dilatancy coefficient, and an enforced stabilising upper bound on the argument of the exponential function in equation (2) – more details provided by Li *et al.* (2024). The formulation refinements related to sand's undrained cyclic behaviour proposed by Liu *et al.* (2020) are not considered in the subsequent monopile analyses, as they are not relevant to the specific problem at hand.

SIMULATION OF PISA CYCLIC TESTS IN SAND

This section covers relevant numerical modelling aspects, including general 3D FE model set-up and SANISAND-MS model calibration for the PISA cyclic tests at Dunkirk. In particular, the piles labelled as DM4 and DM2 are considered, which were subjected to, respectively, monotonic and cyclic lateral loading and feature (McAdam *et al.*, 2020; Byrne *et al.*, 2020b):

- outer diameter $D = 0{\cdot}762$ m
- wall thickness $t = 14$ mm
- embedded length $L = 4$ m (hence $L/D = 5{\cdot}24$)
- load eccentricity above ground level $h_e = 10$ m.

Both piles were installed and laterally loaded in almost identical soil conditions, extensively described by Zdravković *et al.* (2020). To enable fair comparison with existing literature, the same ground model adopted by Taborda *et al.* (2020) was considered for setting up the 3D FE model and calibrate all SANISAND-MS parameters.

GROUND CONDITIONS

The Dunkirk site comprises a dense layer of partially saturated fill material overlaying a sand layer extending from 3 to 30 m below ground surface – the groundwater table is located at a depth of 5·4 m. In the lack of specific characterisation data, the shallow fill material was assumed to share the same mechanical properties of the underlying sand, though with a different relative density – D_r was set equal to 75% (initial void ratio: $e_{ini} = 0{\cdot}628$) and 100% ($e_{ini} = 0{\cdot}54$) for the sand and the fill layer, respectively, with the soil unit weight equal to 17·1 and 19·9 kN/m^3 above and below the groundwater table. Horizontal stresses in the soil were initialised using an estimated earth pressure coefficient (K_0) equal to 0·4. Figure 2 shows a comparison between the profiles of initial pore-water pressure, small-strain shear modulus (G_{max}) and state parameter (ψ) that were set in this study (using PLAXIS 3D 2023.2) and in the study by Taborda *et al.* (2020) (using ICFEP, the Imperial College Finite Element Program) – the minor discrepancy in the upper 4 m may be attributed to slight differences between the two FE programmes in setting up soil's initial conditions (prior to pile installation).

FE MODEL SET-UP

Figure 3 illustrates the 3D FE model built in this study. The symmetry associated with unidirectional lateral loading was exploited for computational convenience, so that only half of the whole problem domain was explicitly modelled. To ensure no boundary effects on the simulated pile response, the soil domain extends 50 m horizontally and has a depth of 12 m. The FE mesh consists of 10 node tetrahedral elements, featuring specific mesh refinement in the vicinity of the pile to capture expected high stress/strain gradients accurately. The lower boundary of the model is fixed, while the side boundaries are constrained to prevent displacement in the normal direction.

The steel pile was modelled as a zero-thickness cylindrical shell and discretised using plate elements, to which Young's modulus and Poisson's ratio equal to 2·11 GPa and 0·3, respectively, were assigned. Zero-thickness interface elements were used to simulate the interaction between soil and structural elements, employing a cohesionless Mohr–Coulomb interface model with both stiffness components (normal and tangential) equal to 10^5 kN/m^3 and friction angle of 32° (Taborda *et al.*, 2020). At individual stress

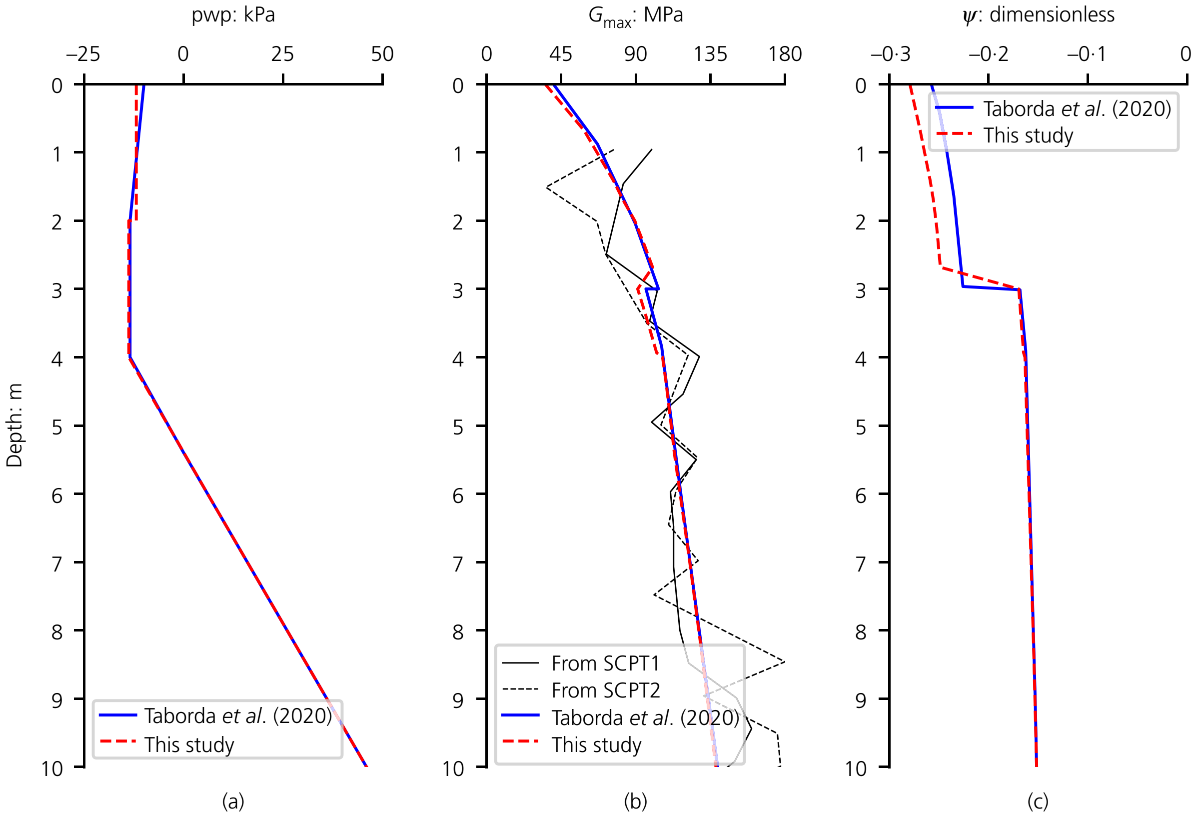

Fig. 2. Initial ground conditions: depth profiles of (left) pore water pressure (pwp), (centre) small-strain shear modulus (G_{max}), (right) state parameters ψ

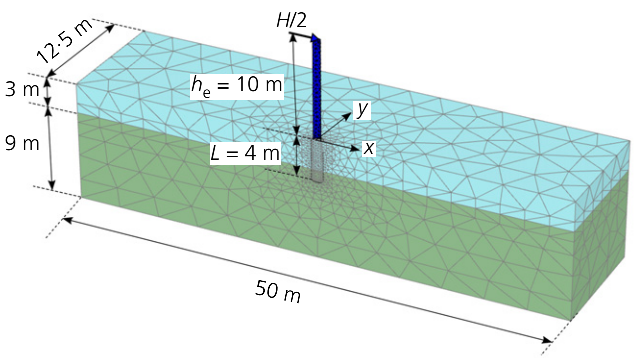

Fig. 3. 3D FE model

points, the soil constitutive equations were integrated using an explicit, third-order Runge–Kutta (RK) scheme with automatic sub-stepping and error control. In comparison to Liu *et al.* (2022a) (where model integration settings are described in more detail), lower-order RK integration (third in lieu of fourth) was enhanced with a drift correction algorithm to guarantee satisfactory efficiency and accuracy.

All FE simulations were executed through combinations of the following phases:

- Step 1: initialisation of effective geo-static stresses, using $K_0 = 0{\cdot}4$.
- Step 2: activation of interfaces and structural elements (with associated material properties).
- Step 3a: static application of prescribed lateral displacement at pile head.
- Step 3b: dynamic application of cyclic load history at pile head.

The monotonic load test on pile DM4 was simulated through the sequence step 1→step 2→step 3a, while the response to cyclic loading of pile DM2 was analysed by replacing step 3a with step 3b. As reported by Byrne *et al.* (2020b), pile DM2 was subjected to a multi-amplitude cyclic loading history comprising five purely one-way load packages, all applied at 0·1 Hz. For each load set (LS) Table 1 reports: maximum applied load (H_{max}), ζ_b ratio between H_{max} and lateral capacity (based on definitions by LeBlanc *et al.*, 2010), number of loading cycles (N).

A growing body of recent research has shown that different pile installation methods may give rise to differences in post-installation lateral response (Fan *et al.*, 2021; Staubach *et al.*, 2021; Kementzetzidis *et al.*, 2023). Although this study focuses on the analysis of lateral pile behaviour through standard 'wished-in-place' modelling (as also done by Taborda *et al.*, 2020), an attempt was made to consider the effects of impact piling using a simplified approach inspired by the study by Broere & van Tol (2006). Accordingly, prior to lateral loading, a planar volumetric expansion ε_{vol}^{inst} (i.e. with nil vertical strain) was applied to the whole soil plug volume up to the interface with the outer soil (thus including the fictitiously nil volume of the pile). In the next section, simulation results accounting for installation effects are always associated with the application of ε_{vol}^{inst} between the aforementioned steps 1 and 2.

CALIBRATION OF SANISAND-MS PARAMETERS

SANISAND-MS, including its monotonic backbone, is primarily derived from the parent model proposed by Dafalias & Manzari (2004), which is similar in many respects to the later bounding surface model developed by Taborda *et al.* (2014). The latter was adopted by Taborda *et al.* (2020) to simulate the PISA field tests conducted in Dunkirk. The

SANISAND-MS parameters that govern the monotonic response are listed in Table 2 (from G_0 to n^d) and were obtained by comparing to the parameter set provided by Taborda *et al.* (2020), though bearing in mind some inevitable differences between the respective model formulations (and the corresponding meaning of material parameters). In the latter regard, it is worth mentioning that:

1. to prevent the attainment of unrealistic soil states, the values of the maximum and minimum void ratios – respectively equal to 0·91 and 0·54 for the Dunkirk sand (Taborda *et al.*, 2020) – were enforced as constraints on the evolution of the void ratio
2. an upper limit equal to 1·63 was set for the stress ratio describing the opening angle of the bounding surface, $M_b = M_c \exp(n^b\psi)$ (Taborda *et al.*, 2020)
3. the dimensionless shear stiffness parameter (G_0 in Table 2) was calibrated to reproduce the small-strain shear modulus (G_{max}) profile obtained from seismic cone penetration test (SCPT) data – Fig. 2 shows close agreement between in situ data, the G_{max} profile considered by Taborda *et al.* (2020) and that adopted herein
4. the SANISAND-MS parameters that are not directly relatable to the formulation of Taborda *et al.* (2014) (e.g. A_0 and h_0 in Table 2) were determined through trial-and-error to match as closely as possible the results of the triaxial test simulations reported by Taborda *et al.* (2020).

Table 1. LS applied to pile DM2

LS (#)	H_{max}: kN	ζ_b: –	N: –
1	10	0·046	5100
2	20	0·093	3300
3	40	0·19	8100
4	80	0·37	11110
11	160	0·74	31

In support of point 4, Fig. 4 shows the comparison between Taborda *et al.* (2020)'s simulation results and those obtained using SANISAND-MS, for triaxial tests conducted on isotropically consolidated samples at different values of initial void ratio and mean effective stress. The comparison in terms of deviatoric stress against axial strain and volumetric strain against axial strain indicates good agreement between the two sets of model simulations, as well as comparable accuracy in reproducing the reference laboratory test results (Taborda *et al.*, 2020).

The calibration of the SANISAND-MS parameters governing cyclic response features, including ratcheting, would ideally require a set of high-cyclic laboratory test data. Such data were provided, for the case of Karlsruhe sand, by Wichtmann (2005) and utilised by Liu *et al.* (2019) to directly calibrate SANISAND-MS. However, the lack of specific high-cyclic characterisation for Dunkirk sand led to adopt an alternative calibration approach. The cyclic parameters μ_0, ζ and β were initially set equal (or similar) to the values identified by Liu *et al.* (2019) for Karlsruhe sand. Subsequently, these parameters were refined using the measured response of the DM2 pile to the first cyclic load set (LS1) reported in Table 1.

COMPARISON TO FIELD DATA

Figure 5 presents a comparison between the measured monotonic response of pile DM4 and the corresponding

Table 2. Dunkirk sand's SANISAND-MS model parameters

Elasticity		Critical state					Yield surface	Plastic modulus			Dilatancy		Memory surface		
G_0	ν	M_c	c	λ_c	e_0	ξ	m	h_0	c_h	n_b	A_0	n_d	μ_0	ζ	β
451	0·17	1·28	0·7188	0·135	0·91	0·179	0·065	3·5	1·0	1·9	1·3	0·75	260	10^{-4}, 10^3	1

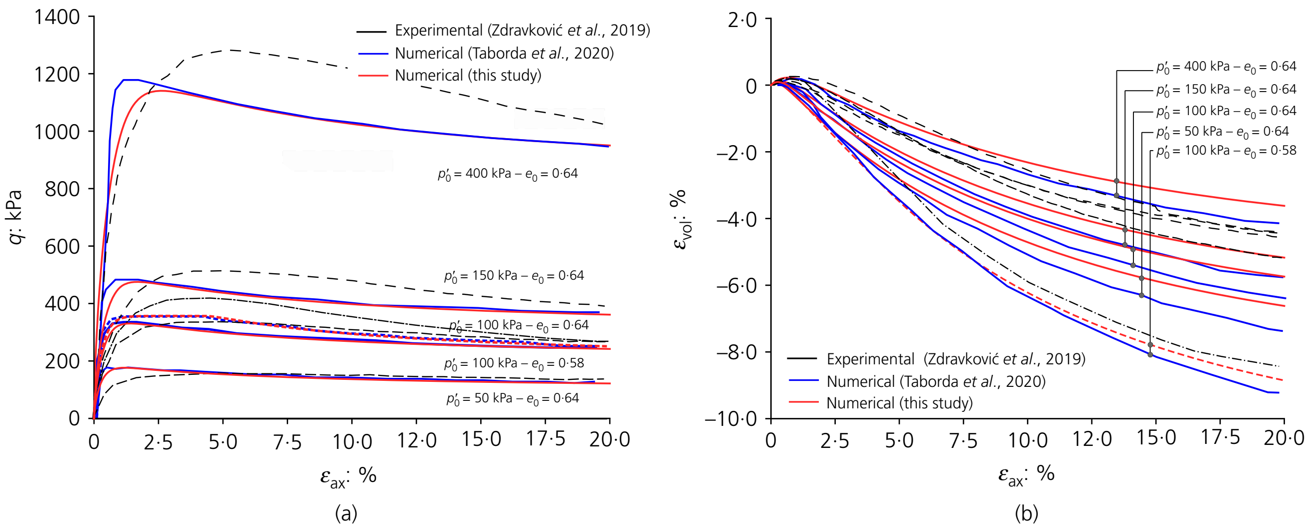

Fig. 4. Simulation of PISA's triaxial tests on Durkirk sand specimens: comparison between model simulations from Taborda *et al.* (2020) and this study: (a) axial strain-deviatoric stress and (b) axial strain-volumetric strain

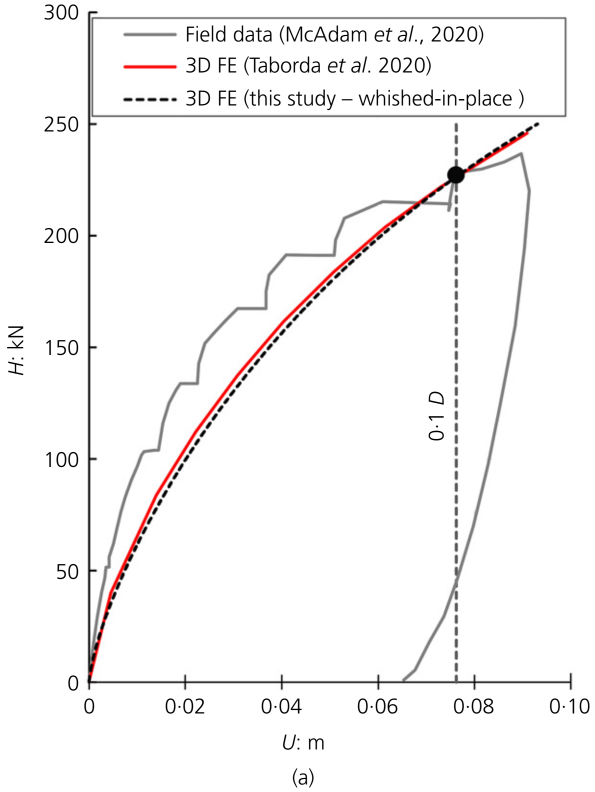

Fig. 5. Monotonic lateral response of pile DM4: comparison between PISA field data and 3D FE simulations from Taborda *et al*. (2020): (a) wished-in-place only and (b) this study (both wished-in-place and with imposed installation strain)

3D FE simulation results from Taborda *et al*. (2020) and this study. The comparison is shown in terms of applied lateral load (H) against pile displacement at ground surface (U). The ultimate lateral capacity of the foundation is conventionally associated with $U = 0{\cdot}1D$, where D is the pile diameter.

Given the similar triaxial test simulations, shown in Fig. 4, the calibrated SANISAND-MS parameters led to 3D FE results that are as close to the reference field data as those obtained by Taborda *et al*. (2020). Since model parameters have been defined by integrating laboratory and in situ data, the 3D FE results appear in Fig. 5a to be rather satisfactory despite the adoption of the simplified wished-in-place approach – confirming the validity of the approach followed by Taborda *et al*. (2020). Particularly, setting the soil's small-strain stiffness solely based on the results of triaxial tests on isotropically consolidated samples (Fig. 2) would have led to further underestimate the lateral small-deflection stiffness of the pile, while better results have been obtained by using a shear modulus profile inferred from SCPTs – see also Kementzetzidis *et al*. (2021). As a further step, improved agreement with the field data at low load levels was achieved by setting an initial installation strain ε_{vol}^{inst} equal to 1%, following the approach by Broere & van Tol (2006) – see Fig. 5(b). In what follows, $\varepsilon_{vol}^{inst} = 1\%$ is regarded as a calibrated, site-specific installation parameter for both piles DM2 and DM4. The impact of ε_{vol}^{inst} on the soil state near the pile is displayed in Fig. 6, which reports the simulated pre- and post-installation profiles of mean effective stress (p'), small-strain shear modulus (G_{max}), memory surface size (m^M) – at a distance of 0·4 m from the vertical pile axis. The profiles shown in the figure indicate that the adopted strategy for reproducing pile installation effects produces a visible enhancement of the soil's mean effective stress near the pile. This enhancement arises from enforcing the lateral expansion of a constrained volume of soil in a manner that approximately captures the effects of pile penetration and determines a stiffer response to monotonic loading (on the other hand, the impact of local void ratio variations was found to be negligible). Following initialisation to the same value as the fixed yield surface size (m in Table 2), the post-installation profile of m^M describes a substantial alteration of the sand's fabric, which is expected to influence the ensuing pile response to lateral cyclic loading.

The same 3D FE model was then employed to simulate the multi-amplitude cyclic test reported by Byrne *et al*. (2020b), in combination with the following cyclic parameter settings (cf. to Table 2):

- μ_0, the main ratcheting-control parameter, was set equal to 260, which is the same value identified for Karlsruhe sand by Liu *et al*. (2019). Such a value was determined with respect to the measured response of the DM2 pile to the first load parcel, LS1, in Table 1.
- The same value $\beta = 1$ adopted by Liu *et al*. (2019) was retained herein. β is known to mostly affect the post-dilation reduction of the mean effective stress during undrained cyclic. On the other hand, Liu *et al*. (2019) also showed the negligible impact of β on drained cyclic strain accumulation, which led to limit the efforts on its calibration for a problem not governed by hydro-mechanical effects (i.e. slow lateral loading of a pile in permeable soil).
- ζ determines the shrinkage rate of the memory surface (fabric damage) when the soil is loaded into its dilative regime. As discussed by Corti *et al*. (2016) and Liu *et al*. (2019), the shrinkage mechanism has a remarkable impact both on drained and undrained cyclic responses,

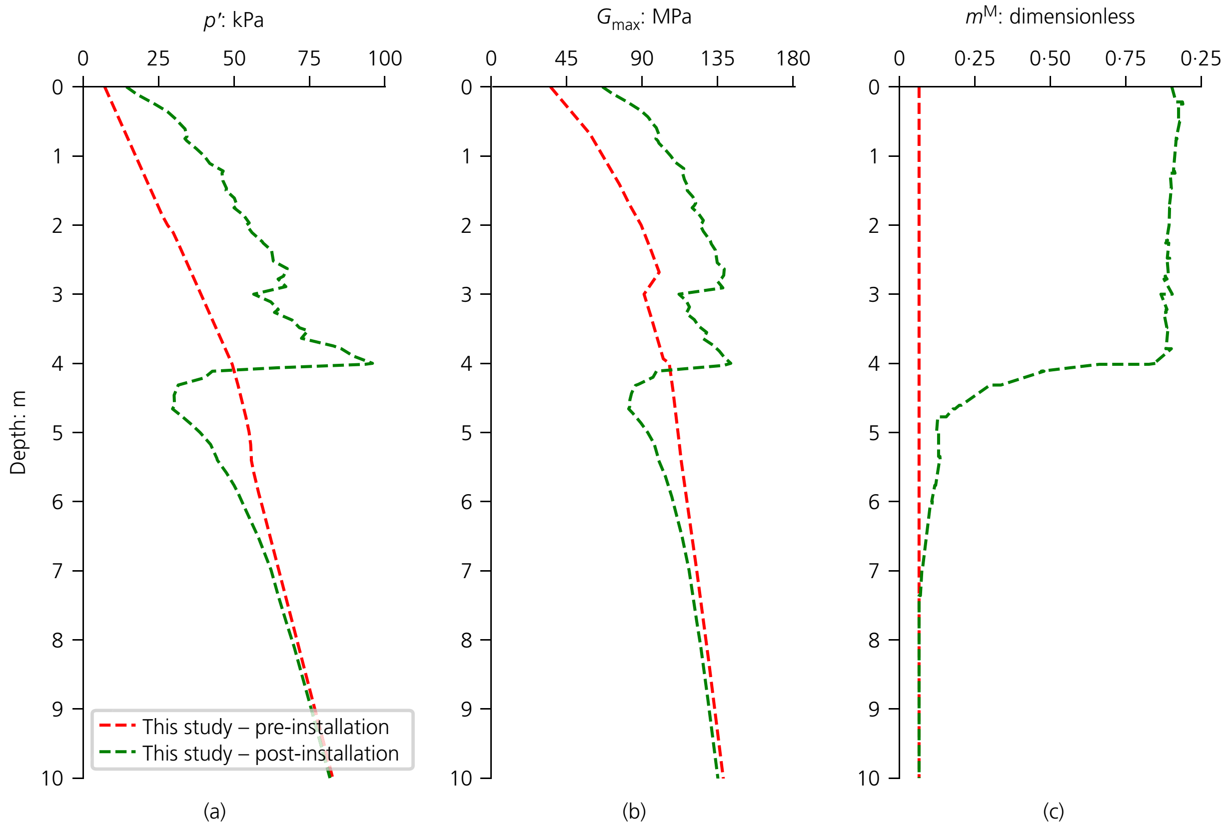

Fig. 6. Simulated pre- and post-installation profiles of (left) mean effective stress (p'), (centre) small-strain shear modulus (G_{max}), (right) memory surface size (m^M)

which may jointly provide input to the calibration of ζ. As pile test data could not straightforwardly support the calibration of ζ, an initial value of 10^{-4} was set (similar to the value identified by Liu *et al.* (2019) for Karlsruhe sand).

The similarities between the cyclic parameters (particularly of the ratcheting-control parameter, μ_0) set for the Dunkirk and Karlsruhe sands may be a posteriori justified in light of Table 3, which provides relevant index properties for the two sands and the parameters of the well-known explicit high-cycle accumulation (HCA) model proposed by Niemunis *et al.* (2005). Further to their similar quartzitic nature, the two sands turned out to be characterised by very similar HCA model parameters, here estimated based on the empirical (and micromechanically based) correlations provided by Wichtmann (2016). Therefore, the two sands may be expected to feature similar cyclic ratcheting properties, in spite of some visible granulometric differences (e.g. in terms of median grain size, D_{50}).

The calibrated 3D FE model produced the results shown in Fig. 7(a), where numerical and experimental $U_R - N$ pile response curves are plotted for the load sets LS1 through LS3.

As shown in Fig. 7(a), U_R indicates the pile head deflection accumulated at ground surface during each jth cycle – note that cycles are counted with respect to the deflection maxima after the initial monotonic load branch, loosely referred to as 0th cycle (LeBlanc *et al.*, 2010). More formally, $U_R = U^i_{j,\max} - U^i_{0,\max}$, where i and j count, respectively, the LS number and the number of cycles within each LS (with $j = 0$ indicating the reference deflection value for obtaining U_R). To limit the computational cost of 3D FE analyses, no more than 100 cycles per LS have been

Table 3. Comparison between Dunkirk and Karlsruhe sands: index properties – from Zdravković *et al.* (2020) and Liu *et al.* (2019) – and estimated HCA model parameters – based on Wichtmann (2016)

Sand	D_{50}: mm	C_U: –	e_{min}: –	e_{min}: –
Dunkirk	0·28	1·72	0·54	0·91
Karlsruhe	0·55	1·8	0·577	0·874

HCA parameters

C_{N-1}: –	C_{N-2}: –	C_{N-3}: –	C_p: –	C_Y: –	C_e: –
$7·7 \times 10^{-4}$	0·15	$5·5 \times 10^{-5}$	0·45	2·4	0·51
$8·1 \times 10^{-4}$	0·14	$6·3 \times 10^{-5}$	0·42	2·6	0·55

simulated. While the good agreement for LS1 is an outcome of the specific μ_0 calibration, it is readily apparent that pile deflection is substantially overestimated for LS2 and LS3, though with reasonable agreement in terms of deflection accumulation rate after the first cycle.

As a subsequent step, simulations were repeated for all five LSs (LS1 through LS5) by including the pile installation effects using Broere & van Tol's approach, with $\varepsilon^{inst}_{vol} = 1\%$. The resulting $U_R - N$ trends in Fig. 7(b) indicate that the changes (stiffening) in soil state associated with pile installation (see post-installation profiles of G_{max} and m^M in Fig. 6) may quantitatively influence cyclic monopile tilt, also in terms of accumulation rate against the number of cycles. On a different note, the model can spontaneously reproduce the increase in accumulation rate resulting from progressively larger ζ_b values (cyclic load amplitude ratio), in a manner not previously pointed out by, for example,

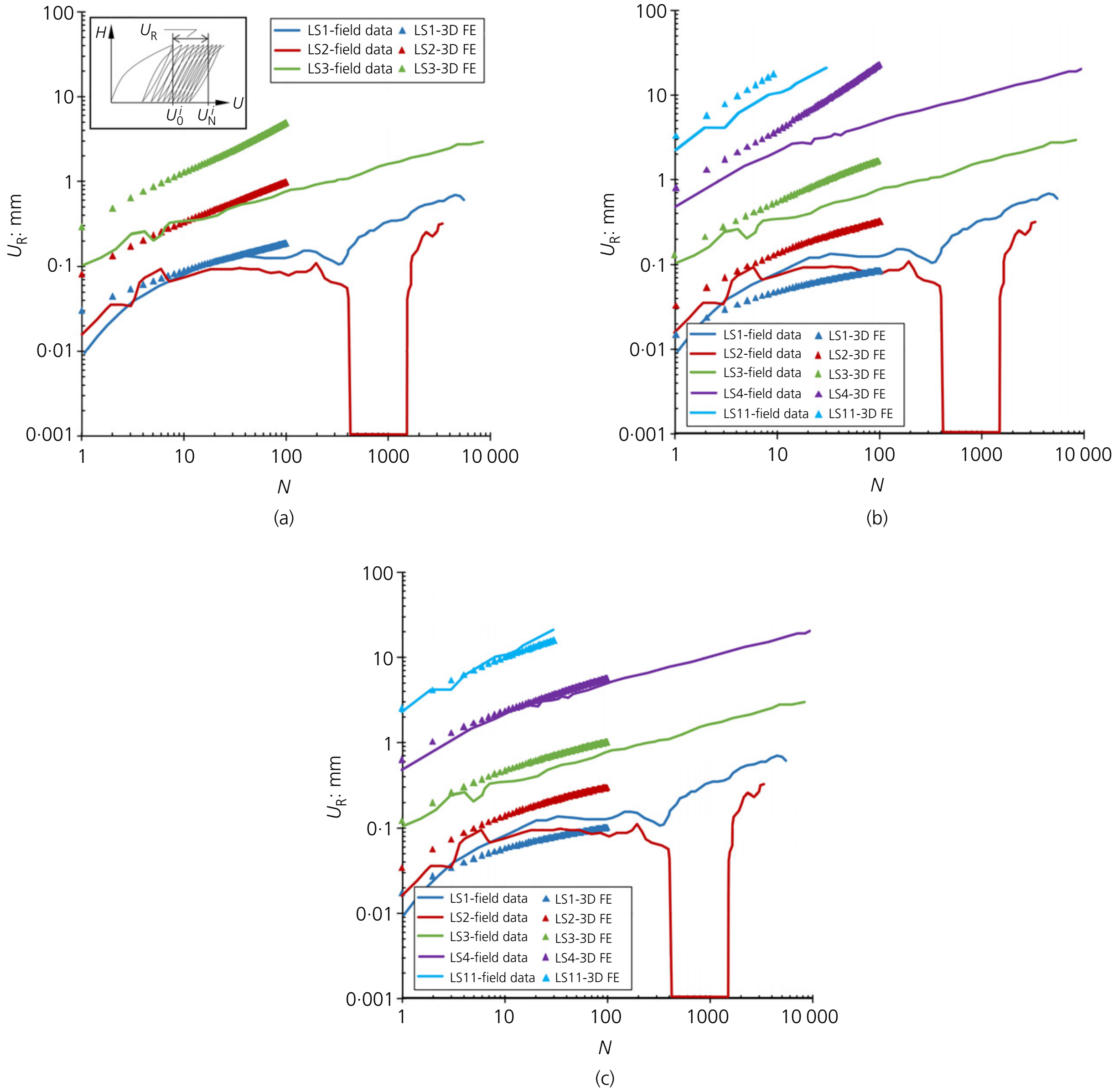

Fig. 7. 3D FE SANISAND-MS simulation of PISA's cyclic test at Dunkirk on pile DM2 – cyclic monopile deflection accumulation at ground surface, experimental data reported by Byrne *et al*. (2020b): (a) with wished-in-place monopile, (b) accounting for monopile installation based on Broere & van Tol (2006) (with ε_{vol}^{inst}= 1%) and (c) accounting for monopile installation and with inhibited memory surface shrinkage (ζ = 10^3)

LeBlanc *et al.*'s experimental investigation (LeBlanc *et al.*, 2010). While it is noted that ζ_b values larger than 0·5 are hardly ever experienced by real monopiles, the results in Fig. 7(b) confirm the good predictive capabilities of the adopted model against real field measurements.

Figure 7(b) also shows an accelerating tilting trend under load package LS4 that is inconsistent with the corresponding measurements. Further consideration of the above calibration assumptions led to recognise that the selected ζ value (= 10^{-4}) may have exaggerated the shrinking mechanism of the memory surface, which would only be noticeable for medium–high cyclic load amplitudes – that is, able to mobilise substantial sand dilatancy (Liu *et al.*, 2019). The results of new numerical simulations with inhibited fabric damage (obtained by setting a sufficiently large ζ value) are reported in Fig. 7(c) and show very encouraging agreement with field data (also after noting that LS2 data probably suffered from some experimental difficulties). This finding implicitly indicates that sand's fabric damage at the microscale may not be a factor governing the cyclic lateral behaviour of monopiles, particularly if pore-pressure build-up may overall be negligible. The dominance of soil ratcheting and densification is not only supported by the reference PISA field data, but also by previous laboratory studies – see, for example, the investigation into high-cyclic monopile behaviour by Cuéllar *et al.* (2012). Similar conclusions are supported by the comparison in Fig. 8 between 3D FE results and the cyclic monopile rotation trends reported by Beuckelaers (2017) for the same field test on pile DM2.

The simulated load–deflection response to the cyclic LSs LS1, LS2, LS3, LS4 and LS11 is presented in Fig. 9. While incorporating gapping effects in the shallow unsaturated soil fell beyond the scope of this study (Kementzetzidis *et al.*, 2023), it is important to note that restricting the numerical simulation to $N \leq 100$ might have limited the degree of realism in simulating the evolution of sand states compared to the field response spanning thousands of load cycles.

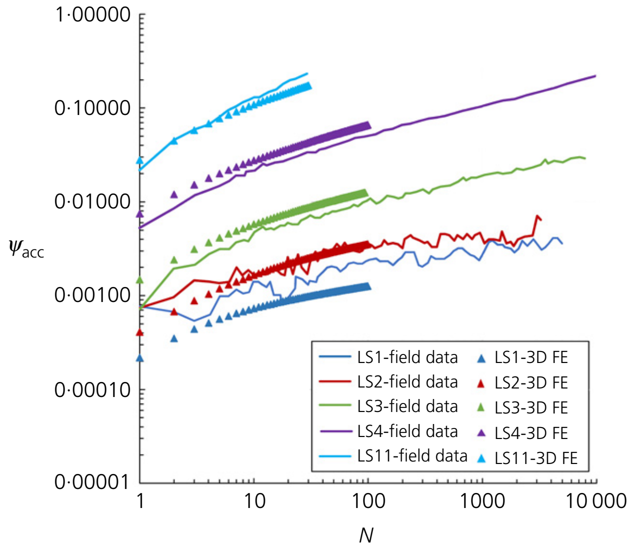

Fig. 8. 3D FE SANISAND-MS simulation of PISA's cyclic test at Dunkirk on pile DM2 – cyclic monopile rotation accumulation at ground surface, experimental data reported by Beuckelaers (2017)

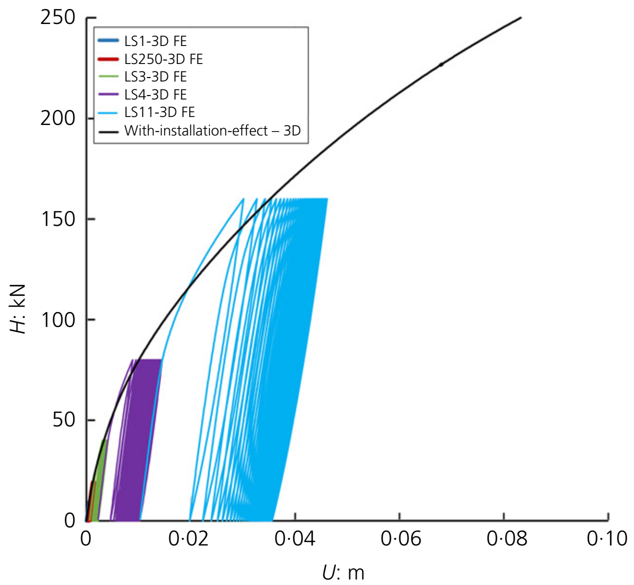

Fig. 9. 3D FE SANISAND-MS simulation of PISA's cyclic test at Dunkirk on pile DM2 – lateral load–deflection response

Nevertheless, the judicious selection of parameters and the simulation of pile installation effects, albeit in a simplified manner, yielded satisfactory 3D FE results. These outcomes support the strengths of the proposed modelling approach.

CONCLUDING REMARKS

This study has presented a 3D FE investigation into the response of monopiles to multi-amplitude cyclic loading in sandy soil. After describing the main features and calibration of the adopted SANISAND-MS model, numerical results have been compared to pile load test data published by the PISA project team after a field testing campaign in Dunkirk (France). To the authors' knowledge, the fully 'implicit' 3D FE simulation of the PISA cyclic tests has been attempted herein for the first time, and has highlighted the following relevant points.

- Pile installation effects should be considered to quantitatively capture cyclic monopile tilt, particularly under the load cycles that immediately follow installation. While such effects have been shown in the literature not to impact the tilt accumulation rate in the long term, they may influence the total permanent rotation and therefore the outcome of monopile tilt assessments. However, additional studies – both experimental and numerical – will be necessary to further explore suitability and precise calibration of the simplified approach adopted herein to mimic installation effects.
- The competition between different microstructural mechanisms in the soil (e.g. ratcheting and densification against fabric damage) has quantitative influence on the monopile cyclic response. Such an influence is expected to become even more pronounced in the presence of strong hydro-mechanical effects and will require further refinement of SANISAND-MS' calibration procedure.
- Although the availability of medium/large-scale pile test data can strongly support model calibration and validation, such data would typically not be available before the monopile design phase. This reaffirms the importance of additional research on the calibration of soil parameters for advanced cyclic constitutive models, such as SANISAND-MS.

It is worth emphasising how 3D FE analyses of the above kind may contribute to the design workflow in real (offshore wind) projects. Although computational costs would typically impose a limited number of load cycles in numerical simulations (e.g. $N < 500 - 1000$), advanced 3D models may enable in-depth analysis of cyclic monopile behaviour at selected (sometimes problematic) turbine locations. Such detailed studies may be performed to assess the impact of uncertain, yet very relevant, factors, such as specific features of soil behaviour (influence of density and stiffness assumptions, proneness to cyclic ratcheting, drainage conditions), cyclic load conditions and foundation geometry. However, additional efforts should be made to enhance calibration procedures for cyclic constitutive models. This may be accomplished by (*a*) including high-cyclic tests in laboratory test programmes and (*b*) devising empirical correlations between model parameters and commonly available soil data (index properties and in situ test results). Gaining experience in calibrating non-standard soil parameters will benefit practical applications, as in this study the existing SANISAND-MS calibration for Karlsruhe sand has supported the identification of Dunkirk sand's cyclic parameters. In conclusion, it is also worth recalling the option of combining implicit and explicit 3D FE calculations – that is, by using the former to identify cyclic strain levels within the soil and the latter to extrapolate the system response to thousand/million cycles with a much lower computational burden (Staubach & Wichtmann, 2020). However, while this approach would be well applicable to cyclic load histories with regular amplitude packages (as in the PISA test considered herein), its application to random cycling would require rainflow counting and introduce uncertainties regarding load sequence effects (Liu *et al.*, 2022b).

DATA AVAILABILITY STATEMENT

Some or all data used are available from the corresponding author on request.

ACKNOWLEDGEMENTS

The contribution of Zheng Li (TU Delft) and Dr. Haoyuan Liu (NGI) to the numerical implementation of the SANISAND-MS model is very gratefully acknowledged.

REFERENCES

Achmus, M., Kuo, Y. S. & Abdel-Rahman, K. (2009). Behavior of monopile foundations under cyclic lateral load. *Comput. Geotech.* **36**, No. 5, 725–735.

Achmus, M., Schmoor, K. A., Herwig, V. & Matlock, B. (2020). Lateral bearing behaviour of vibro- and impact-driven large-diameter piles in dense sand. *Geotechnik* **43**, No. 3, 147–159.

Been, K. & Jefferies, M. G. (1985). A state parameter for sands. *Géotechnique* **35**, No. 2, 99–112, https://doi.org/10.1680/geot.1985.35.2.99.

Beuckelaers, W. (2017). *Numerical modelling of laterally loaded piles for offshore wind turbines.* PhD thesis, University of Oxford, Oxford, UK.

Broere, W. & van Tol, A. F. (2006). Modelling the bearing capacity of displacement piles in sand. *Proc. Inst. Civil Engng Geotech. Engng* **159**, No. 3, 195–206.

Burd, H. J., Taborda, D. M. G., Zdravković, L., Abadie, C. N., Byrne, B. W., Houlsby, G. T., Gavin, K. G., Igoe, D. J. P., Jardine, R. J., Martin, C. M., McAdam, R. A., Pedro, A. M. G. & Potts, D. M. (2020). PISA design model for monopiles for offshore wind turbines: application to a marine sand. *Géotechnique* **70**, No. 11, 1048–1066, https://doi.org/10.1680/jgeot.18.P.277.

Byrne, T., Gavin, K., Prendergast, L., Cachim, P., Doherty, P. & Pulukul, S. C. (2018). Performance of CPT-based methods to assess monopile driveability in North Sea sands. *Ocean Engng* **166**, 76–91.

Byrne, B. W., Burd, H. J., Zdravković, L., Abadie, C. N., Houlsby, G. T., Jardine, R. J., Martin, C. M., McAdam, R. A., Pacheco Andrade, M., Pedro, A. M. G., Potts, D. M. & Taborda, D. M. G. (2019). PISA design methods for offshore wind turbine monopiles. In *Offshore technology conference, OnePetro.* Houston, TX, USA: Offshore Technology Conference (OTC).

Byrne, B. W., Aghakouchak, A., Buckley, R. M., Burd, H. J., Gengenbach, J., Houlsby, G. T., McAdam, R. A., Martin, C. M., Schranz, F., Sheil, B. B. & Suryasentana, S. K. (2020a). PICASO: cyclic lateral loading of offshore wind turbine monopiles. In *Frontiers in offshore geotechnics IV: proceedings of the 4th international symposium on frontiers in offshore geotechnics (ISFOG 2021)* (ed. Z. J. Westgate), pp. 1526–1535. Austin, TX, USA.

Byrne, B. W., McAdam, R. A., Beuckelaers, W. J. A. P., Burd, H. J., Gavin, K. G., Houlsby, G. T., Igoe, D. J. P., Jardine, R. J., Martin, C. M., Potts, D. M., Taborda, D. M. G. & Zdravković, L. (2020b). Cyclic laterally loaded medium scale field pile testing for the PISA project. In *4th International symposium on frontiers in offshore geotechnics* (ed. Z. J. Westgate), pp. 1323–1332. Austin, TX, USA.

Corti, R., Diambra, A., Wood, D. M., Escribano, D. E. & Nash, D. F. (2016). Memory surface hardening model for granular soils under repeated loading conditions. *J. Engng Mech.* **142**, No. 12, 04016102.

Cuéllar, P., Georgi, S., Baeßler, M. & Rücker, W. (2012). On the quasi-static granular convective flow and sand densification around pile foundations under cyclic lateral loading. *Gran. Matter* **14**, 11–25.

Dafalias, Y. F. & Manzari, M. T. (2004). Simple plasticity sand model accounting for fabric change effects. *J. Engng Mech.* **130**, No. 6, 622–634.

Fan, S., Bienen, B. & Randolph, M. F. (2021). Effects of monopile installation on subsequent lateral response in sand. ii: lateral loading. *J. Geotech. Geoenviron. Engng* **147**, No. 5, 04021022.

Jardine, R., Kontoe, S., Byrne, B., Buckley, R. & McAdam, R. (2019). Research to improve the design of driven pile foundations in chalk: the ALPACA project. *Coast. Struct.* **2019**, 923–930.

Jeanjean, P., Zakeri, A., Zhang, Y. & Andersen, K. H. (2022). The new ISO/API py curves in clays and their reconciliation with the PISA framework. In *Offshore technology conference, OnePetro.* Houston, TX, USA: Offshore Technology Conference (OTC).

Kaynia, A. M. (2019). Seismic considerations in design of offshore wind turbines. *Soil Dyn. Earthquake Engn* **124**, 399–407.

Kementzetzidis, E., Metrikine, A. V., Versteijlen, W. G. & Pisanò, F. (2021). Frequency effects in the dynamic lateral stiffness of monopiles in sand: insight from field tests and 3D FE modelling. *Géotechnique* **71**, No. 9, 812–825, https://doi.org/10.1680/jgeot.19.TI.024.

Kementzetzidis, E., Pisanò, F., Tsetas, A. & Metrikine, A. V. (2023). Gentle driving of piles at a sandy site combining axial and torsional vibrations: quantifying the influence of pile installation method on lateral behavior. *J. Geotech. Geoenviron. Engng* **149**, No. 11, 04023102.

Klinkvort, R., Black, J., Bayton, S., Haigh, S., Madabhushi, G., Blanc, M., Thorel, L., Zania, V., Bienen, B. & Gaudin, C. (2018). A review of modelling effects in centrifuge monopile testing in sand. *Phys. Model. Geotech.* **1**, 720–723.

LeBlanc, C., Houlsby, G. & Byrne, B. (2010). Response of stiff piles in sand to long-term cyclic lateral loading. *Géotechnique* **60**, No. 2, 79–90, https://doi.org/10.1680/geot.7.00196.

Li, Z., Liu, H., Hicks, M. A. & Pisanò, F. (2023). Influence of static–cyclic load misalignment on the drained tilting response of offshore monopiles in sand. *Comput. Geotech.* **156**, 105306.

Li, Z., Del Brocco, I., Hicks, M. A., Brasile, S. & Pisanò, F. (2024). Enhancing the robustness of SANISAND-MS model implementation for implicit cyclic analysis of foundations, in preparation.

Liu, H. & Pisanò, F. (2019). Prediction of oedometer terminal densities through a memory-enhanced cyclic model for sand. *Géotechnique Lett.* **9**, No. 2, 81–88.

Liu, H. Y., Abell, J. A., Diambra, A. & Pisanò, F. (2019). Modelling the cyclic ratcheting of sands through memory-enhanced bounding surface plasticity. *Géotechnique* **69**, No. 9, 783–800, https://doi.org/10.1680/jgeot.17.P.307.

Liu, H., Diambra, A., Abell, J. A. & Pisanò, F. (2020). Memory-enhanced plasticity modeling of sand behavior under undrained cyclic loading. *J. Geotech. Geoenviron. Engng* **146**, No. 11, 04020122.

Liu, H., Kementzetzidis, E., Abell, J. A. & Pisanò, F. (2022a). From cyclic sand ratcheting to tilt accumulation of offshore monopiles: 3D FE modelling using SANISAND-MS. *Géotechnique* **72**, No. 9, 753–768, https://doi.org/10.1680/jgeot.20.P.029.

Liu, H., Pisanò, F., Jostad, H. P. & Sivasithamparam, N. (2022b). Impact of cyclic strain accumulation on the tilting behaviour of monopiles in sand: an assessment of the Miner's rule based on SANISAND-MS 3D FE modelling. *Ocean Engng.* **146**, No. 11, 110579.

Maatouk, S., Blanc, M. & Thorel, L. (2022). Effect of embedding depth on the monotonic lateral response of monopiles in sand: centrifuge and numerical modelling. *Géotechnique* 1–16, https://doi.org/10.1680/jgeot.22.00149.

McAdam, R. A., Byrne, B. W., Houlsby, G. T., Beuckelaers, W. A. P., Burd, H. J., Gavin, K. G., Igoe, D. J. P., Jardine, R. J., Martin, C. M., Muir Wood, A., Potts, D. M., Gretlund, J. S., Taborda, D. M. G. & Zdravković, L. (2020). Monotonic laterally loaded pile testing in a dense marine sand at Dunkirk. *Géotechnique* **70**, No. 11, 986–998, https://doi.org/10.1680/jgeot.18.PISA.004.

Niemunis, A., Wichtmann, T. & Triantafyllidis, T. (2005). A high-cycle accumulation model for sand. *Comput. Geotech.* **32**, No. 4, 245–263.

Page, A. M., Klinkvort, R. T., Bayton, S., Zhang, Y. & Jostad, H. P. (2021). A procedure for predicting the permanent rotation of monopiles in sand supporting offshore wind turbines. *Mar. Struct.* **75**, 102813.

Panagoulias, S., de Winter, C., Navalkar, S. & Nernheim, A. (2023). Sensitivity of the seismic response of monopile-supported offshore wind turbines to soil variability. *Ocean Engng.* **268**, 113545.

Pisanò, F. (2019). Input of advanced geotechnical modelling to the design of offshore wind turbine foundations. In *Proceedings of the 17th European conference on soil mechanics and geotechnical engineering (ECSMGE 2019)* (eds H. Sigursteinsson, S. Erlingsson and B. Bessason), pp. 272–297. London, UK: International Society of Soil Mechanics and Geotechnical Engineering.

Pisanò, F., Askarinejad, A., Wang, H., Maghsoodi, S., Gavin, K. G., Segeren, M. L. A., Elkadi, A. S. K., de Lange, D. & Konstadinou, M. (2022). MIDAS: monopile improved design through advanced cyclic soil modelling. In *Proceedings of the 20th international conference on soil mechanics and geotechnical engineering (ICSMGE2022)*, Sydney, Australia (eds M. Rahman and M. Jaska), pp. 2677–2683. Australian Geomechanics Society.

Pisanò, F., Panagoulias, S., Anastasopoulos, I., Kaynia, A., Petalas, A., Brasile, S., Page, A., Kementzetzidis, E. & Metrikine, A. V. (2024). DONISIS: Design of offshore moNopiles including seismic interaction with soil. *Jpn. Geotech. Soc. Spec. Publ.*, **10**, No. 36, 1383–1388, https://doi.org/10.3208/jgssp.v10.OS-25-05.

Staubach, P. & Wichtmann, T. (2020). Long-term deformations of monopile foundations for offshore wind turbines studied with a high-cycle accumulation model. *Comput. Geotech.* **124**, 103553.

Staubach, P., Machaček, J. & Wichtmann, T. (2021). Large-deformation analysis of pile installation with subsequent lateral loading: Sanisand vs. Hypoplasticity. *Soil Dyn. Earthquake Engn* **151**, 106964.

Staubach, P., Machaček, J., Tafili, M. & Wichtmann, T. (2022). A high-cycle accumulation model for clay and its application to monopile foundations. *Acta Geotech.* **17**, No. 3, 677–698.

Taborda, D., Zdravković, L., Kontoe, S. & Potts, D. (2014). Computational study on the modification of a bounding surface plasticity model for sands. *Comput. Geotech.* **59**, 145–160.

Taborda, D. M. G., Zdravković, L., Potts, D. M., Burd, H. J., Byrne, B. W., Gavin, K. G., Houlsby, G. T., Jardine, R. J., Liu, T., Martin, C. M. & McAdam, R. A. (2020). Finite-element modelling of laterally loaded piles in a dense marine sand at Dunkirk. *Géotechnique* **70**, No. 11, 1014–1029, https://doi.org/10.1680/jgeot.18.PISA.006.

Van Eekelen, H. (1980). Isotropic yield surfaces in three dimensions for use in soil mechanics. *Int. J. Numer. Anal. Methods Geomech.* **4**, No. 1, 89–101.

Westgate, Z. J., DeGroot, D. J., McMullin, C., Zou, Y., Guo, D., Van Haren, S., Beemer, R. D., Zeppilli, D., Miller, K. G. & Browning, J. V. (2023). Effect of degradation on geotechnical behavior of glauconite sands from the US Mid-Atlantic Coastal Plain. *Ocean Engng* **283**, 115081.

Wichtmann, T. (2005). *Explicit accumulation model for non-cohesive soils under cyclic loading*. PhD thesis, Inst. für Grundbau und Bodenmechanik Braunschweig, Karlsruhe, Germany.

Wichtmann, T. (2016). *Soil behaviour under cyclic loading – experimental observations, constitutive description and applications.* Habilitation thesis, Inst. für Grundbau und Bodenmechanik Braunschweig, Karlsruhe, Germany.

Zdravković, L., Jardine, R. J., Taborda, D. M. G., Abadias, D., Burd, H. J., Byrne, B. W., Gavin, K. G., Houlsby, G. T., Igoe, D. J. P., Liu, T., Martin, C. M., McAdam, R. A., Muir Wood, A., Potts, D. M., Gretlund, J. S. & Ushev, E. (2020). Ground characterisation for PISA pile testing and analysis. *Géotechnique* **70**, No. 11, 945–960, https://doi.org/10.1680/jgeot.18.PISA.001.

HOW CAN YOU CONTRIBUTE?

To discuss this paper, please submit up to 500 words to the editor at support@emerald.com. Your contribution will be forwarded to the author(s) for a reply and, if considered appropriate by the editorial board, it will be published as a discussion in a future issue of the journal.